In-lab X-ray fluorescence and diffraction techniques for pathological calcifications

Stéphan Rouzière, Dominique Bazin, Michel Daudon

In-lab X-ray Fluorescence and Diffraction Techniques for Pathological Calcifications

S. Rouzière[a], D. Bazin[a,b], M. Daudon[c,d,e]

[a]Laboratoire de Physique des Solides, UMR CNRS 8502, Bâtiment 510, Université Paris-Sud, 91405 Orsay Cedex, France.
[b]CNRS-LCMCP-Sorbonne Universités - UPMC, Collège de France, Paris, France
[c]Sorbonne Universités, UPMC Univ Paris 06, UMR S 702, Paris, France,
[d]INSERM, UMR S 702, Paris, France,
[e]Explorations Fonctionnelles Multidisciplinaires, AP-HP, Hôpital Tenon, Paris, France,

Corresponding author: Dr. S. Rouzière, **stephan.rouziere@u-psud.fr**

Keywords: In-lab X-ray Fluorescence; In-lab X-ray Diffraction; Diagnosis; Urolithiasis

Abstract: If imaging by physical methods is probably the best well-known link between physics and medicine, other ways such as X-ray fluorescence and diffraction techniques give significant information to clinician. In this contribution, we would like to assess different results obtained through such technique on three main problems in urology namely Randall's plaque, brushite kidney stones and phase conversion between weddellite and whewellite. Randall's plaque is a mineral deposit at the surface of the renal papilla which is responsible for the prevalence increase of kidney stones among young people. X-ray fluorescence suggests that an inflammation process is related to Randall's plaque. X-ray fluorescence shows that brushite stones, well known to be related to some pathologies or biochemical disorders could also be related to unexpected conditions as suggested, for example, by high content of Br found in several brushite stones. Such results deserve further investigations to explain the origin of that element in the stones. Regarding the phase conversion from weddellite to whewellite, X-ray fluorescence data suggest that trace elements initially present in the stone remain for the major part in situ during the conversion process, which may be clinically relevant to relate crystalline phase and etiology. Beginning of answers through X-Ray fluorescence and diffraction techniques are given to the clinicians. These examples as well as other investigations assessed in this contribution underline a typical scientific transfer between a physics laboratory and hospital.

1. Introduction

Since its discovery, X-ray related techniques has gained wide acceptance in materials science. Among them, X-ray fluorescence (XRF) [1-4] and X-ray diffraction (XRD) [5-8] are two well-established and powerful tools for a non-destructive analysis of materials with broad applications in science and industry. In medicine, numerous investigations of biological entities have also been performed with these techniques [9-15]. It is also possible to combine both XRF and XRD on the same experimental set-up to obtain simultaneously elemental and structural information on the sample. Furthermore, technical developments in X-ray laboratory sources, optics and detectors in the recent years have allowed performing measurements at a local scale with micrometric X-ray beams (~10µm in diameter) to investigate possible heterogeneities. The fact that such measurements combining XRF and XRD are now available in the laboratory offers a significant advantage, albeit the weaker X-ray intensity, over similar experiments on synchrotron radiation facilities for which experimental access is scarce. XRD and XRF techniques can also be implemented at the hospital to help to characterize pathologies or for disease diagnosis through in vivo experiments [16].

In this contribution, we would like to underline through different kinds of XRF and XRD experiments, that chemical and structural characteristics of pathological calcifications [17-19] give to clinician invaluable information. For example, most of XRF experiments in medicine deal with trace elements which are intrinsic components of numerous biological systems, since a third of all known proteins contain metal cofactors as catalytic components [20]. Moreover, some trace elements are directly related to a specific disease (aluminum to Alzheimer's disease [21]; copper accumulation to Wilson disease [22]) or are present in therapeutic drugs or diagnostic agents (Cis-platin in chemotherapy [23], gadolinum in magnetic resonance imaging [24] as well different kinds of nanoparticles [25]). After a brief description of the principles of XRF and XRD techniques, we will present a set of experimental data collected on such in-lab facilities.

2. Basics of XRD and XRF techniques

2.1. Interaction of X-rays with matter

X-rays considered as an electromagnetic radiation possess the duality of being both electromagnetic waves with short wavelength λ ranging typically from 0.1 to 1 Å and massless non-charged particles named photons with energies E from 1 to 100 keV. X-ray photons can interact with the electrons in matter by three different mechanisms as shown in figure 1: (i) the photo-electric effect when matter absorbs the incident X-ray photon and then emits electrons or X-ray photons, (ii) Compton scattering, where the scattering of the incident X-ray photon is accompanied by some energy transfer to the electron (inelastic scattering) and (iii) Thomson (elastic) scattering where the scattered X-ray photons have the same energy as in the incident beam. Note that at low energy, the photoelectric effect is more important than Compton scattering.

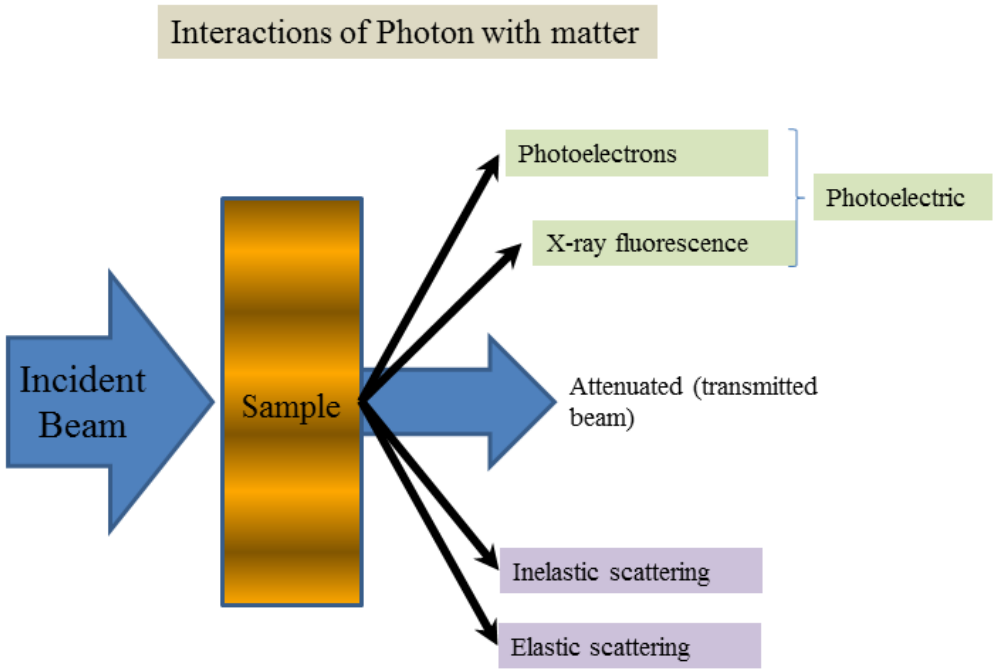

Fig.1. Schematic representation of the different interactions between X-rays and matter.

The photo-electric effect is responsible for the XRF and Auger photoelectrons phenomena whereas XRD is related to Thomson scattering process. Note that photoelectron spectroscopy is usually subdivided according to the source of exciting radiation into X-ray Photoelectron Spectroscopy (XPS) which uses soft x-rays (with a photon energy of 200-2000 eV) to examine core-levels and Ultraviolet Photoelectron Spectroscopy (UPS) which is based on UV radiation (with a photon energy of 10-45 eV) to examine valence levels.

2.2. X-ray fluorescence

In the photoelectric absorption process, incident photons with quantum energy ($h\nu$) interact with an absorber atom and completely disappear. In their place, photoelectrons are ejected from one of the bound shells of the atom with energy equal to $h\nu - E_b$ (where E_b represents the binding energy of the photoelectron in its original shell, see figure 2a). During the atomic relaxation, the filling of the inner shell vacancy can produce X-ray fluorescence radiation with characteristic energies of the atom and also other photoelectrons named Auger electrons [26, 27].

The characteristic energies of the X-ray fluorescence radiation emitted from a sample enable to identify unambiguously and quantify the different elements present. Such experiment can be performed on solid, liquid or thin-film samples. Finally, note that X-ray fluorescence can be also induced by gamma-emitting radioisotopes (^{241}Am, ^{109}Cd, ^{153}Gd, and others), protons [28-31], electron sources and synchrotron light sources which produce highly intense, coherent, monochromatic X-ray beams [32-36].

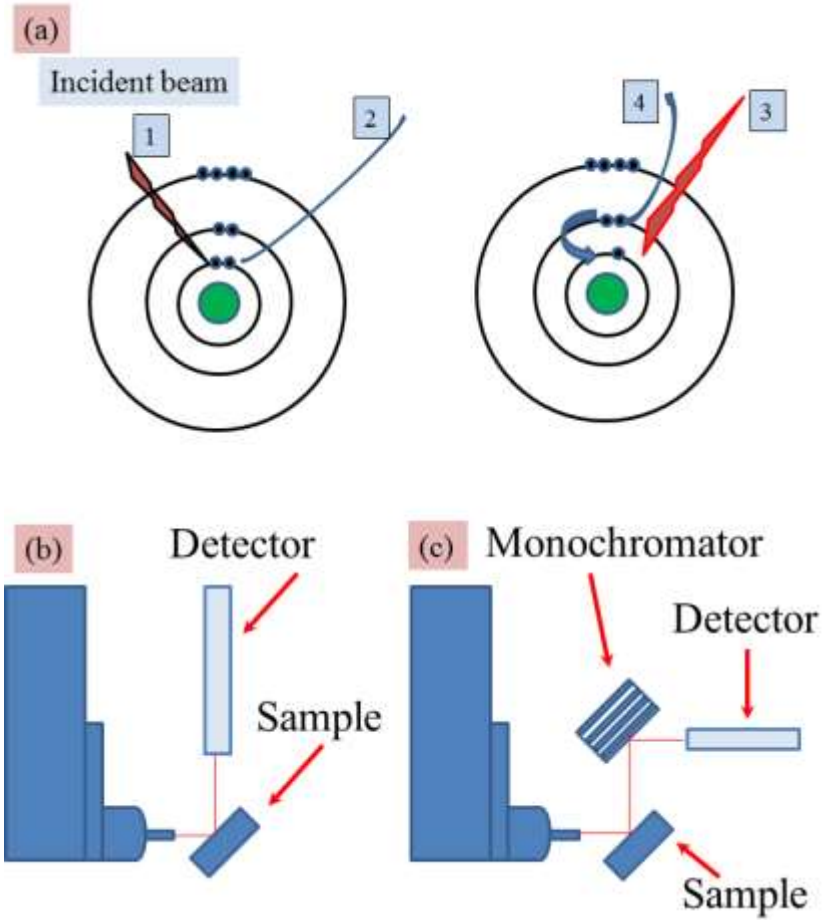

Fig.2. (a) Simple representation associated with the X-ray fluorescence process: 1- incident X-ray photon, 2- emitted photoelectron, 3- X-ray fluorescence photon or 4- Auger electron (b,c) Schematic experimental set-ups corresponding to (b) energy-dispersive (ED) and (c) wavelength-dispersive (WD). For the ED experimental device, the energy resolution is given by the detector (around 150-200eV) while for the WD one, the energy resolution is defined by the monochromator (around 1-2 eV).

XRF can be in general measured with two types of experimental set-ups: (i) energy-dispersive (ED-XRF) and (ii) wavelength-dispersive (WD-XRF) spectrometers (Fig. 2b). In the latter, the fluorescence radiation is diffracted by an analysing single crystal optic just after the sample to select with a high sensitivity a very narrow wavelength or characteristic energy from an element of interest in the sample. In the ED-XRF mode, the detector allows to detect simultaneously a broad range of characteristic energies possibly related to several elements, the selectivity depending on the energy resolution and counting rate performance of the detector.

Laboratory X-ray sources must provide sufficiently high energy radiation to be able to excite the characteristic energies of the broadest range of elements of the periodic table; they are electric generators producing X-rays emission radiation from a high-Z element anode like molybdenum, silver or tungsten. X-ray optics, crystalline monochromator or multilayer mirror, is coupled with the generator to deliver a focusing monochromatic beam onto the

sample that greatly improve signal-to-noise ratio for measurements of the characteristic energies of elements present in the sample (Fig. 3a).

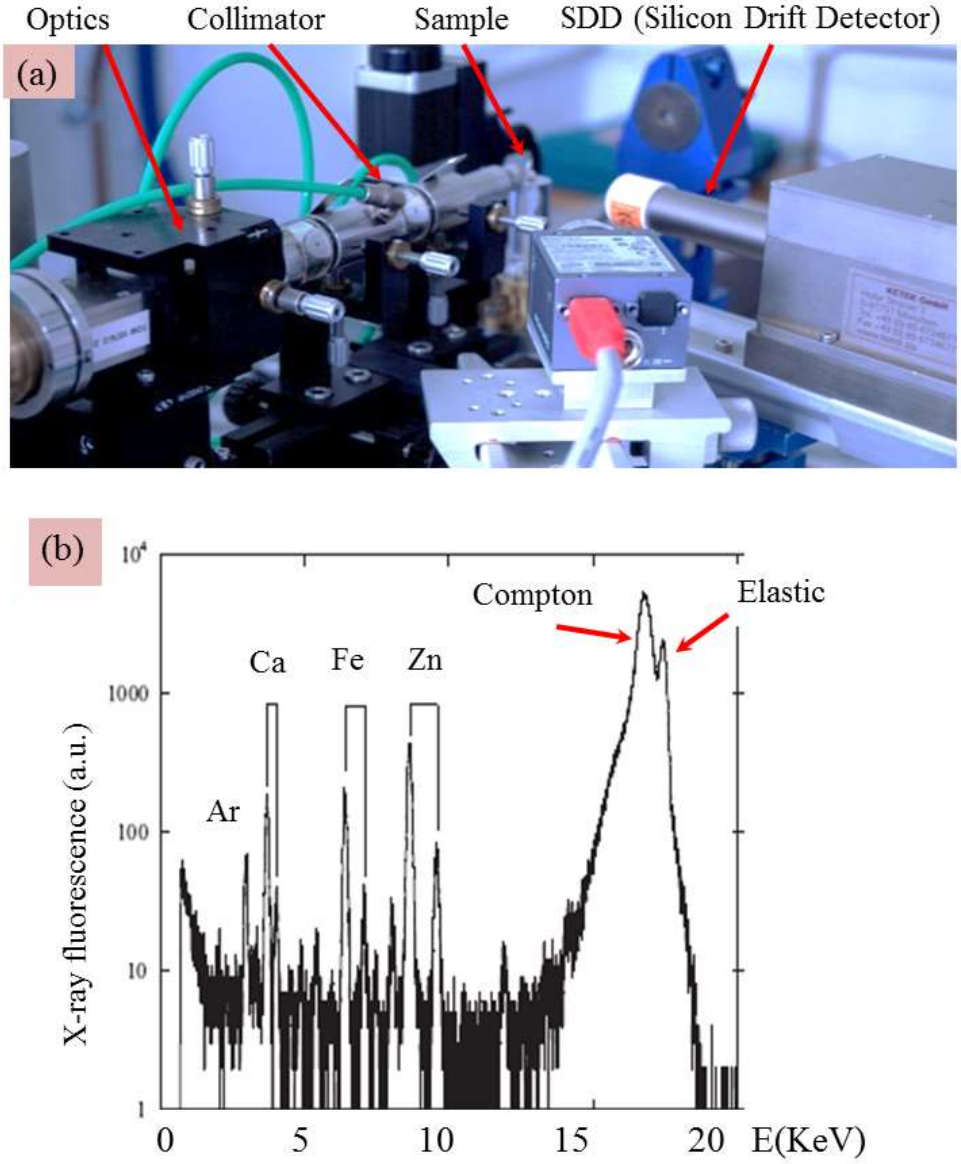

Fig.3. (a) Picture of in-lab EDXRF experimental set-up at LPS with monochromatic X-ray MoK_α radiation, the different elements are indicated by arrows (b) typical X-ray fluorescence measured for a pathological calcification (a kidney stone). The contributions of trace elements such Fe and Zn are clearly visible.

On figure 3b, we can see clearly the contributions of Ar (K_α= 2958 eV), Ca (K_α= 3691 eV, K_β= 4012 eV), Fe (K_α= 6404 eV, K_β= 7058 eV) and Zn (K_α= 8638 eV, K_β= 9572 eV). Other contributions exist coming from inelastic process (Compton scattering) as well as the elastic scattering related to the energy of the incident photons generated by the molybdenum anode. Finally, the absence of signal at low energy (typically elements below Al) cannot contribute to the spectrum due to air absorption, the high difference between the incident energy of the Mo-K_α and the binding energy of the electrons of low Z elements which induces

a low probability of photoionization, and the out-of-range (below 1 keV) sensitivity of the silicon drift detector.

XRF is a representative multi-element technique for the analysis of trace elements. This technique constitutes a simple and rapid procedure of analysis for a large number of samples, high sensitivity and low-detection limits, enabling the determination of elements concentrations in trace level.

2.3. X-ray diffraction

At the atomic level, each atom of the sample defines a scattered wave built from an incident X-ray beam. Wavelengths of X-rays being of the order of inter-atomic distances in the matter, the spatial periodic configuration of atoms causes phase interferences between scattered waves, thus giving rise to the diffraction pattern. XRD was discovered in 1913 by von Laue and by Bragg father and son [37] who established the well-known Bragg formula, $2d \sin \theta = n\lambda$ (n is a positive integer), which connects the wavelength λ of the incident X-rays, the atomic lattice interplanar distance d and the deviation angles θ corresponding to the constructive interferences of scattered waves. From an experimental point of view, the XRD pattern is measured through a collection of diffraction peaks at different Bragg angles 2θ, their angular positions and their intensities being intimately related to the spatial arrangement of the atoms.

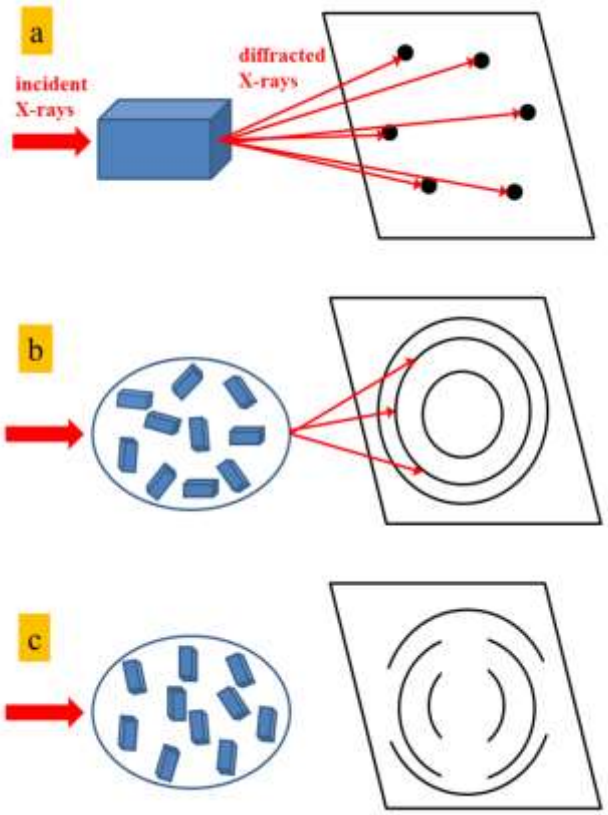

Fig.4. Schematic representation of the diffraction patterns on a plane detector from a single crystal (a), a polycrystalline powder (b) and a preferential orientated powder (c).

On figure 4, the different cases of diffraction from a single crystal (long range order periodic atomic arrangement), a polycrystalline powder (random orientation of small crystals) and a powder of crystallites with a preferential orientation (texture) are shown to illustrate the corresponding diffraction patterns. XRD can bring different kinds of information on the sample such as the identification of the crystallographic phases, its microstructure or its texture [38-41]. Generally, XRD is used for phase identification by comparing the values of diffracted peaks with the ones tabulated in a data base [42] and can also determine the structure of new compounds. Recently, we have observed stone formation in rats subjected to diets containing l-choline tartrate. Using powder and single-crystal XRD, it is possible to determine the crystallographic structure of completely new chemical phase [43-45]. It is also possible to follow the formation and reactivity of a phase or observing changes in lattice constants under stress/change as, for example, to study prosthesis under mechanical stress [46-50].

2.4 In-lab micro- XRD and XRF

X-ray micro-diffraction (µXRD) is well adapted to investigate the local variations of crystallographic properties such as the crystalline phase identification, the microstructure or the preferential orientation. It is also valuable to combine such structural information with a local elemental analysis by µXRF. The main concern to perform experiments at a micrometric scale on a lab X-ray source is to obtain an X-ray microbeam sufficiently intense. Recent developments of instrumentation in X-ray optics and detectors allow optimizing the detection of low-intensity signals with a monochromatic CuK_α X-ray microbeam with dimensions typically of 20 µm in diameter [51].

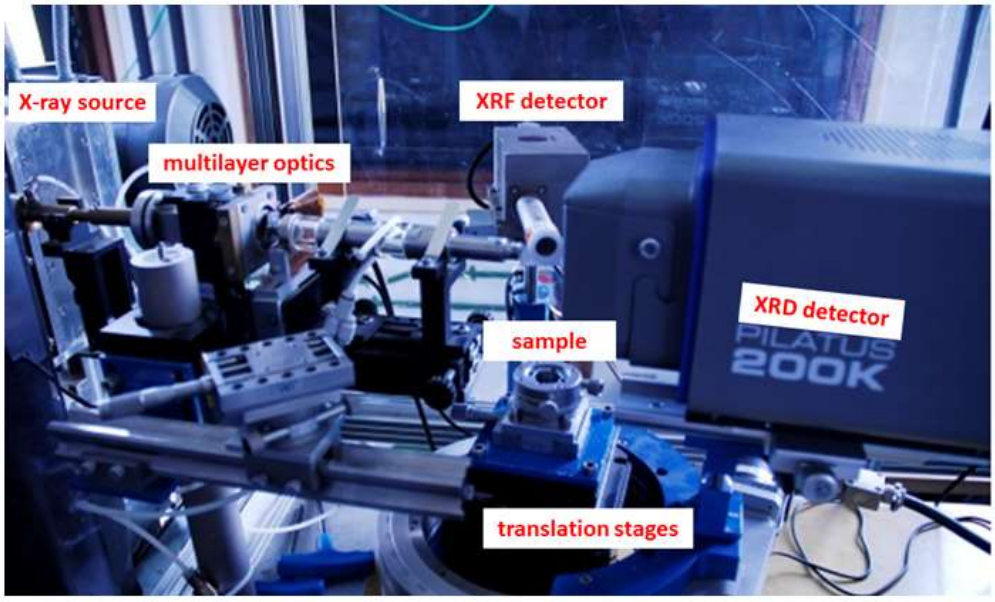

Fig.5. Picture of the in-lab µXRD/µXRF instrument at LPS with monochromatic X-ray CuK_α radiation, the different elements of the setup are indicated.

On figure 5, the experimental setup includes a multilayer mirror associated with a high-brilliance rotating-anode generator delivering a well-defined beam of sufficient intensity to measure µXRD and µXRF signals within a short time (time scale from 1 to 10 minutes according to the sample studied). Detectors using recently developed technology, such as hybrid-pixel detectors are well suited to measure the low-intensity signals. High resolution motorized translation stages allow performing area mapping studies on materials.

3. Randall's plaque, XRD and XRF

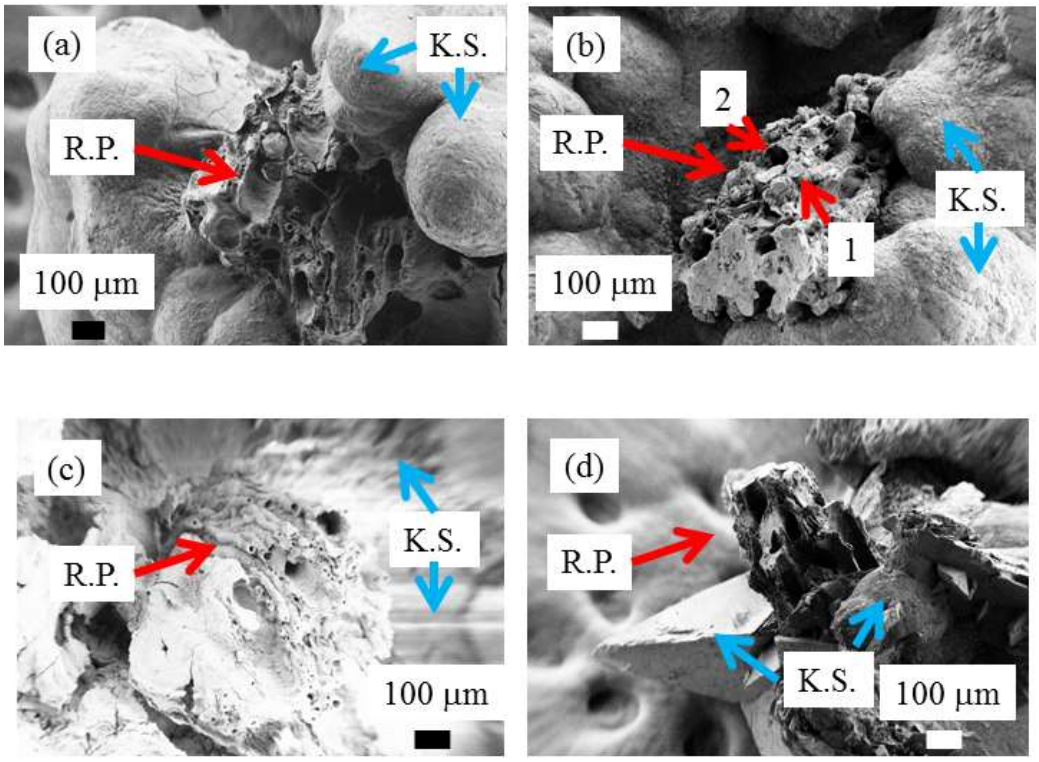

Fig.6. Randall's plaques observed at the mesoscopic scale. (a,b,c) Randall's plaques made of calcium phosphate apatite (RP, red arrows) are positioned on kidney stone (KS, blue arrows) constituted of calcium oxalate monohydrate. Calcium phosphate apatite can be present within the tubular lumen (1 in b), while other tubules are empty with calcified walls (2 in b). In some cases (d), Randall's plaque are found at the surface of kidney stones made of calcium oxalate dehydrate (KS, blue arrows).

Crystallization may be induced in metastable supersaturated solutions by spontaneous nucleation when a certain degree of supersaturation is reached (homogeneous nucleation) or by an additional support made of seed crystals or polymeric substances (heterogeneous nucleation). One of the main challenges for urology in the 21st century is related to a heterogeneous nucleation namely the Randall's plaque (RP) [52-55]. These subepithelial calcifications of the renal papilla (figure 6) act as an anchor for calcium oxalate monohydrate crystals and considerable efforts have been made over the last decades to identify the biochemical parameters responsible for this ectopic calcification [56-65]. More precisely, a

detailed description of the interface area between a RP and a whewellite ($CaC_2O_4.H_2O$, calcium oxalate monohydrate, COM) stone at the mesoscopic scale shows randomly distributed COM crystals trapped in the carbonated apatite of RP [17]. S.C. Kim et al. [66] have observed that stone formation is in fact proportional to papillary surface coverage by RP. It is also worthwhile to note that such calcification of the renal papilla may eventually become large enough to occlude the tubular lumina and obliterate the tubular epithelium [67].

This deposit is also present at the surface of kidney stones [68, 69]. In that case, even if other phosphate phases such as whitlockite or brushite can be found as minor components (less than 5%), calcium phosphate apatite (CA) as well as amorphous carbonated calcium phosphate (ACCP) are the major components of most RPs. In order to improve our knowledge on the chemical composition of RP present at the tip of the papilla, we use a technique specific to synchrotron radiation namely, X-ray absorption spectroscopy [70, 71]. Such technique had already been used in several investigations regarding pathological and physiological calcifications [72-76]. In the case of Randall's plaque, such experiments give for the first time direct structural evidence of the presence of ACCP as a major constituent [77].

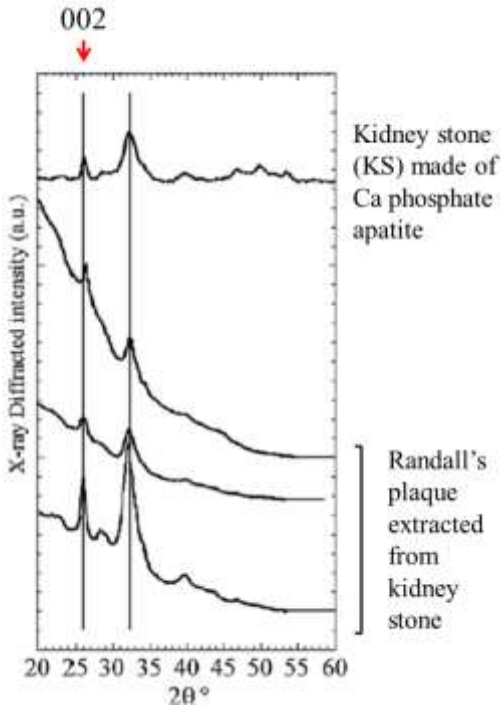

Fig.7. X-ray diffraction diagrams collected with monochromatic copper radiation (λ =1.542Å) for different RP and a KS made of apatite used as a biological apatite reference sample in this study (after ref. 78). Measurements were performed with an X-ray photosensitive image plate.

Based on these previous achievements, we have performed XRD and XRF experiments on a set of RP extracted using a stereomicroscope from seven human KS and one kidney stone made of calcium phosphate apatite (used in this study as a reference compound) [78]. As it can be observed in figure 7, XRD diagrams correspond to a relatively fine (002) diffraction peak (at 2θ=26◦) and several poorly resolved lines constituting a broad peak

between 2θ=30◦ and 2θ=35◦. From these observations, it is quite easy to conclude that RP are made of nanocrystalline particles displaying the usual anisotropy along the c axis [79-84].

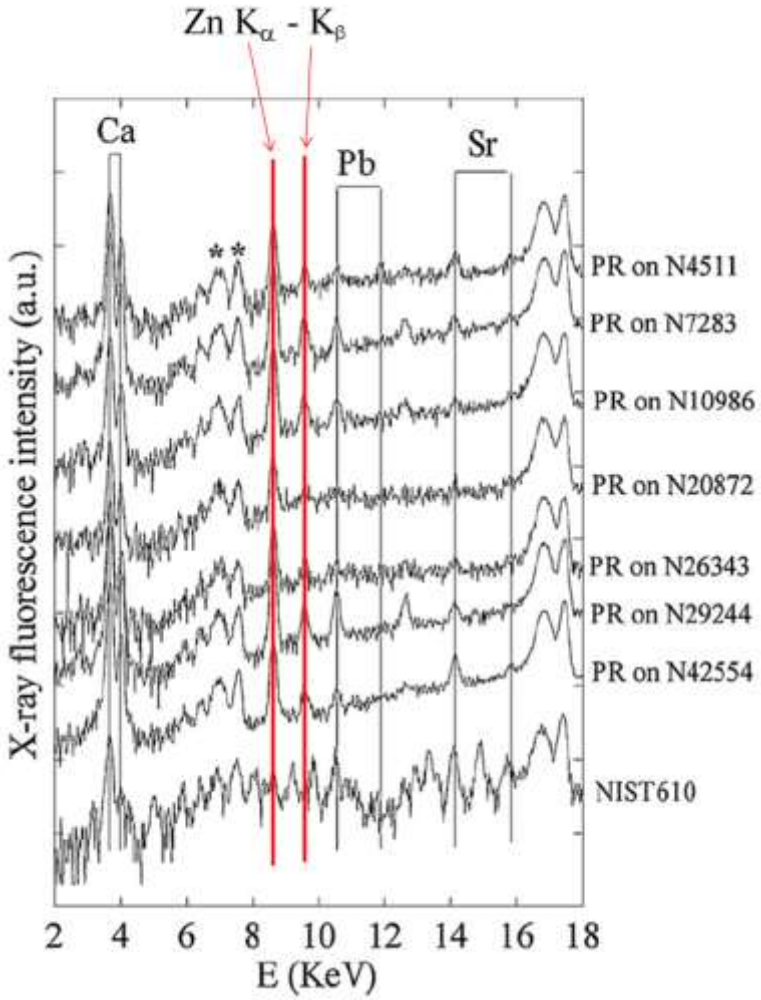

Fig.8. Typical X-ray fluorescence spectra collected for RP and calibration compound NIST610. For RP, we can clearly see the contributions of Ca (EK_α= 3.691 keV, EK_β = 4.012 keV), Zn (EK_α = 8.638 keV, EK_β= 9.572 keV), Pb (EL_α= 10.551 keV, EL_β= 12.613 keV) and Sr (E_α=14.165 keV, EK_β=15.835 keV) (after ref 78). Measurement was performed with a germanium detector.

More interesting results have been collected by XRF (figure 8). The contributions of different trace elements such as Zn, Pb and Sr have been measured. These elements have divalent cations and ionic radius close to the one of Ca^{2+} in line with the Goldschmitt rules which are associated to insertion processes [85]. Such data are in line with the fact that apatitic calcium phosphates offer a wide range of ion substitutions which can modify the physical–chemical and biological properties of apatites [86-88]. The quantitative analysis provides evidence that Zn levels are dramatically increased in RP by comparison to the ones corresponding to kidney stones of the same composition. The amount of Zn (μg/g) is between 15 and 32 in kidney tissue, around 0.1 in urine, 1000 in CA kidney stones compared to 5600 in RP (up to 10,000 in some cases) [78]. Such high level of Zn suggests that calcified deposits

within the medullar interstitium are clearly a pathological process involving a tissue reaction in agreement with the decrease of the kidney function [79-93].

4. Hyperoxaluria, hypercalciuria and XRF

As reported for a long time, weddellite ($CaC_2O_4.2H_2O$, Calcium oxalate dehydrate) is mainly related to hypercalciuria while whewellite is associated with hyperoxaluria [94,95]. In a previous investigation [33], we have noticed that Zn and Sr content were higher in weddellite (290µg/g and 125µg/g respectively) than in whewellite (42µg/g and 61µg/g respectively) stones, suggesting significant differences in the urine, including its content of Zn and Sr, which is known to follow calcium pathways, seems to be increased in kidney stones associated with hypercalciuric states [33]. A simple question arises: what is the Zn content in kidney stones made of whewellite for which a phase conversion has occurred, considering that crystalline conversion is observed for weddellite, which is able to transform to whewellite. Crystalline conversion is suspected when the morphological type of the stone is type II, typical for weddellite structure with large specific bipyramidal crystals while the infrared spectrum clearly demonstrates that whewellite is the main component of the corresponding areas of the stone. By contrast, stones initially made of whewellite exhibit a type I morphology, very useful for assessing hyperoxaluric states as a driving force of stone formation. In the case of crystalline conversion, the initial stone morphology is preserved for a long time, allowing easy detection of a conversion process by comparison between morphology and composition of the stone. Because crystalline conversion from weddellite to whewellite implies a dissolution-crystallization process, it was expected that all stones mainly composed of whewellite, irrespective to the initial phase, should contain significantly less Zn and Sr than weddellite stones. To answer this question, a new set of measurements have been performed (Table 1). The ratio calculated from the areas of the respective fluorescence peaks of each element allows carrying a semi-quantitative analysis to compare the relative ratio of two elements in each sample. As we can see, even if a large modulation of the Zn/Ca ratio is observed in this series, the statistical analysis of these measurements is able to distinguish between native whewellite and whewellite coming from weddellite as assessed by the morphology of the stones. Studies based on XRF confirm our first results suggesting a different biological environment for whewellite and weddellite crystallization, weddellite being associated to a Zn-rich environment, partly favoured by an inflammation process [33, 96]. Thus, whewellite resulting from weddellite conversion by a dissolution-crystallization process (type II morphology) preserves the initial environment and presents a high content of Zn (and at a less extent strontium) by comparison to native whewellite (type I morphology). The Ca/Zn and Ca/Sr ratios were respectively 16.1 ± 43.8 and 4.6 ± 7.5 for weddellite versus 300.8 ± 28.3 and 29.3 ± 4.9 for whewellite ($p = 0.000053$ for Ca/Zn and $p = 0.015$ for Ca/Sr). It could be of interest to assess the relative ability of Zn and Sr adsorption and/or absorption on weddellite and whewellite crystals in *in vitro* experiments of synthesis of weddellite or whewellite crystals. As observed in table 1, stone morphology compared with stone composition determined by infrared spectroscopy helps to identify crystalline conversion and thus stone aetiology.

Table 1.

Zn/Ca ratio obtained from calculated areas of the fluorescence peaks of Ca (K_α + K_β) and Zn (K_α) measured by XRF for different Calcium oxalate kidney stones. (Wh : whewellite; Wd: Weddellite; CA: calcium phosphate apatite; Prot: proteins: WK: Whitlockite). Note that ratio values are not molar quantity.

Stone reference	Ca/Zn	Ca/Sr	Sex	Morphological type of the stone surface	Morphological type of the stone section	Stone composition (number values are indicated in %)
68316	9.9	0.9	M	IIb	IIb+IVa	Wh 60+CA 21+Wd 15+Prot 4
56486	14.9	9.3	M	IIa+IVa	IIb+IVa	Wd 44+CA 30+Wh 20+Prot 6
68076	15.6	2.08	M	IIb	IIb	Wh 52+Wd 40+CA 5+Br 3
68285	19.2	10	M	IIb	IIb	Wd 56+Wh 35+CA 7+Prot 2
68351	20.8	0.86	M	IIb+IVa	IIb+IVa	Wd 36+CA 32+Wh 28+Prot 4
68114	110	7.8	F	IIb+Ia	Ia+IIb	Wh 50+Wd 45+CA 3+Prot 2
68097	176	26	M	IIb+Id	Ia+IIb	Wh 80+Wd 11+CA 6+Prot 3
57503	230	10.8	M	Ie	Ie	Wh 100
68096	240	16.6	M	Ia	Ia	Wh 100
68231	261	30	F	IIb+IVb+Ia	Ia	Wh 36+Wd 26+CA 25+WK 10+Prot 3
68074	272	23.9	M	Ia+IIb	Ia	Wh 65+Wd 30+CA 3+Prot 2
68214	286	39	F	Ia	Ia	Wh 100
8624	328	78	F	Ia	Ia	Wh 100
68140	380	7.9	M	Ia+IIb	Ia	Wh 64+Wd 28+CA 4+Prot 4
60982	380	38	M	Ie	Ie	Wh 100
68102	410	30	F	Ia	Ia	Wh 96+CA 2+Prot 2
68258	537	43	M	Ia>IIb	Ia	Wh 80+Wd 15+CA 3+Prot 2

5. Brushite and X-ray fluorescence

Brushite (dicalcium phosphate dihydrate, $CaHPO_4,2H_2O$), named after the American mineralogist George Jarvis Brush (1831 -1912), [97] is a chemical compound which has a pivotal role in medicine. Brushite as well as octacalcium phosphate and amorphous calcium phosphate apatite have been proposed as the earliest solid calcium phosphate phase deposited in bone [98]. This is due to the fact that if brushite is more stable than hydroxyl-apatite in sufficiently acid solution, brushite hydrolyzes directly into hydroxyl-apatite at sufficiently basic pH [99]. Brushite is also used in prosthesis to improve the corrosion resistance and biocompatibility of metallic alloys [100,101] or in cement implants for bone regeneration [102,103]. Finally, brushite can be identified in different pathological calcifications [104,105].

In urology, the main problem of brushite stones is their resistance to fragmentation through extracorporeal shockwave lithotripsy [106]. Through micro computerized tomography, it has been shown that resistance roughly correlates with stone density and increases with the brushite mineral content, which is consistent with clinical experience regarding patients with brushite calculi [107]. The fact that multiple lithotripsy sessions in a patient give rise to the pathogenesis of brushite stones has been also assessed [108,109].

D. Ackermann et al. [110] report that the state of saturation towards brushite was exclusively determined by urinary calcium and pH, the latter below 5.5 showing a high influence on brushite solubility. As underlined by C.Y. Pak et al. [111], patients with predominantly brushite stones could be distinguished from those with predominantly hydroxyapatite and calcium oxalate stones by higher urinary supersaturation with respect to brushite due mainly to hypercalciuria from absorptive hypercalciuria. Finally, R. Siener et al. [112] noticed that hypercalciuria, a diminished citrate excretion and an elevated pH turned out to be the major urinary determinants of brushite stone formation. Finally, in urine

Brushite is the most acidic form of calcium phosphates identified in urine and stones. While carbapatite is a very common component of urinary calculi, identified in various proportions in about 85% of all stones, brushite is much less frequent and is observed in less than 5% of urinary stones. One explanation could be that brushite is considered an instable phase of calcium phosphate able to transform with time to carbapatite [113]. However, the occurrence of brushite was increasing since the past three decades. In addition, the sex ratio found for stone formers producing brushite stones is dramatically different than that observed for carbapatite stones (ratio H/F=3.08 for brushite and 0.68 for carbapatite stones, $p < 0.00001$). Finally, the strong relation between brushite and some pathological states or biochemical disorders suggests that brushite could have a special place in nephrolithiasis. In fact, in contrast with carbapatite, brushite is strongly linked to hypercalciuric states (87% of patients producing brushite stones exhibit hypercalciuria) [114].

Moreover, among well-defined metabolic diseases, primary hyperparathyroidism is especially frequent in the case of brushite stones (close to 20% of cases). Other causes may be considered such as urinary tract infection, medullary sponge kidney, phosphate leak, mellitus diabetes or tubular acidification defect. However, these pathological conditions often induce

mixed calcium phosphate stones also containing high proportions of carbapatite. It seems that multiple biochemical disorders as poorly acidic urine pH, high calcium, high phosphate and low citrate concentration and/or excretion are required for brushite stone formation [114].
Based on the well-established correlation between stone morphology and pathology [115-119] for COM [115] and for some types of carbapatite stones [65], we examined brushite stone morphology and the content of the main trace elements by comparison with the calcium content. Four groups of brushite stones were selected according to the pathology: primary hyperparathyroidism (n=8), hypercalciuria (n=7), mellitus diabetes (n=4) and urinary tract infection (n=8). At the macroscopic and mesoscopic scales, it was not possible to distinguish between all these pathologies from stone morphology or crystallites morphology assessed by SEM examination. To illustrate this difficulty, crystallites morphology through a field emission scanning electron microscope (FE-SEM) implemented at the Laboratoire de Physique des Solides (LPS) of brushite kidney stones is shown in figure 9.

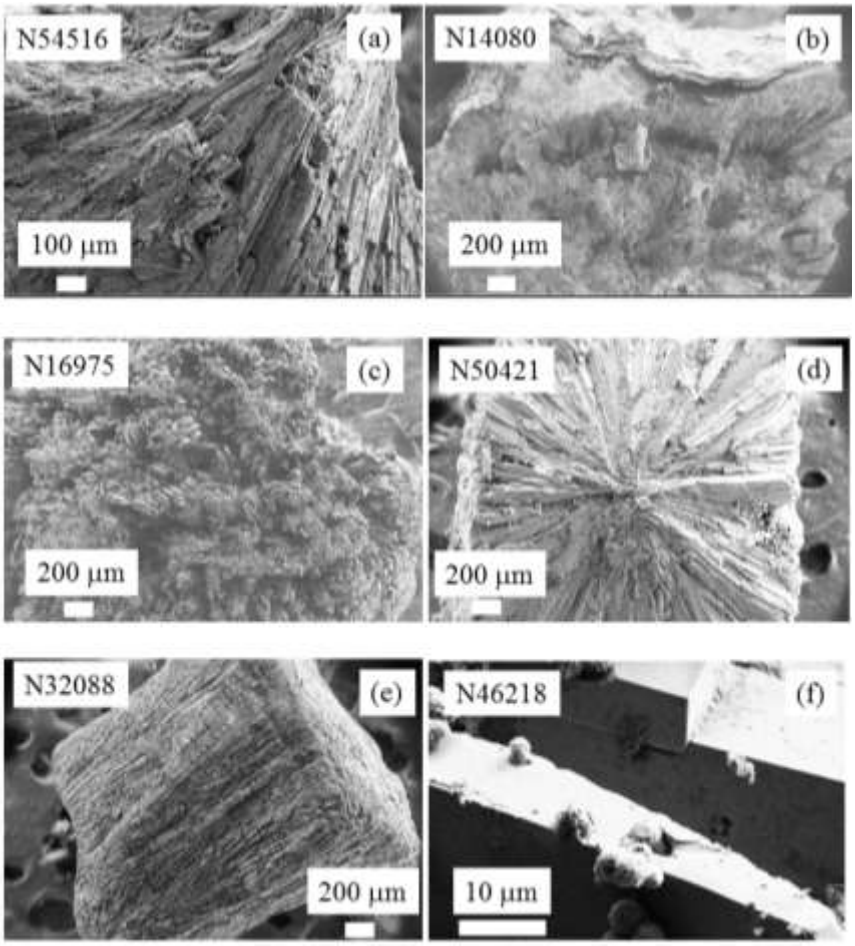

Fig.9. FE SEM photographs of brushite kidney stones. These observations show clearly that brushite kidney stones may display very different morphologies. Unfortunately it was not possible to relate a specific morphology to a particular disease (i.e. primary hyperparathyroidism, hypercalciuria, mellitus diabetes, urinary tract infection). (f) Phase transition between brushite and apatite observed at a high magnification

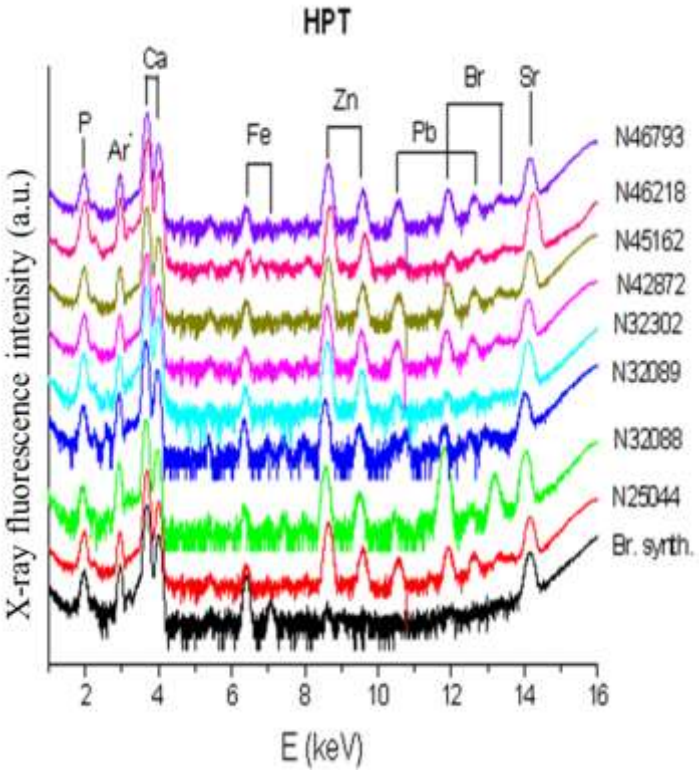

Fig.10. X-ray fluorescence spectra collected for brushite kidney stones related to primary hyperparathyroidism (HPT). The X-ray fluorescence coming from Ar is due to the fact that measurements are performed in the ambient pressure.

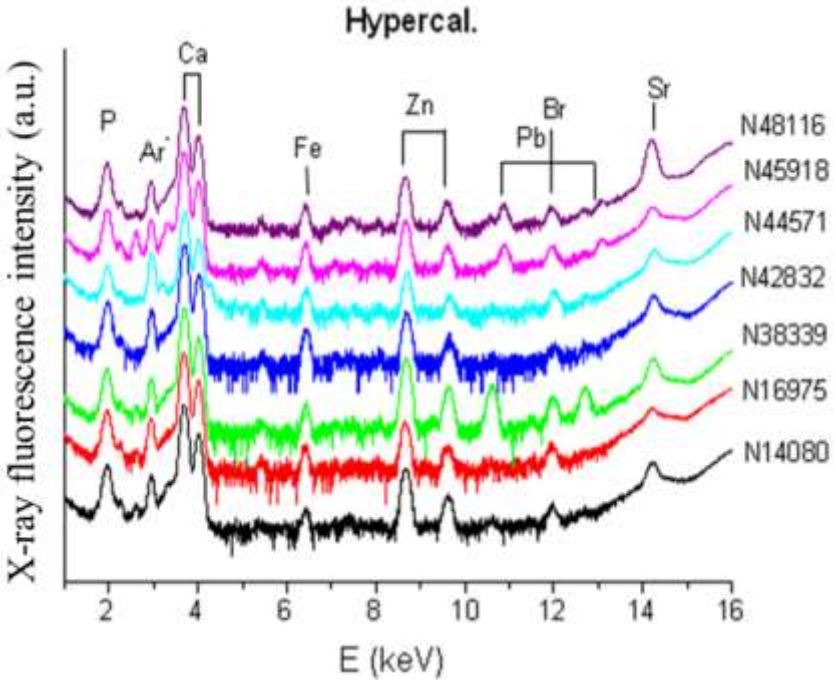

Fig.11. X-ray fluorescence spectra collected for brushite kidney stones related to hypercalciuria.

Trace elements identified by X-ray fluorescence (figure 10 and 11) were Br, Pb, Sr, Zn and Fe. The results were expressed as the ratio of each element to the calcium content (Table 2). Our data failed to find any difference between groups as concern the ratio Sr/Ca or Br/Ca. In contrast, we observed that the Zn/Ca ratio was significantly higher in stones from diabetic patients by comparison to hypercalciuria (0.0704 ±0.0108 vs 0.0253 ± 0.008 ($p < 0.01$). These data suggest that other factors than hypercalciuria (often present also in diabetic patients because a defect in calcium reabsorption) could explain the high content in Zn. Especially, inflammatory process could be involved in those patients [120,121]. Of note, the presence, and sometimes the relatively high content of Br in several brushite stones remains unexplained and deserves further investigation.

Table 2.
Zn/Ca ratio obtained from the fluorescence of Ca (K_α + K_β) and Zn (K_α) measured by XRF (counting acquisition of 20mn for each spectrum) for different brushite kidney stones related to hyperparathyroidism, hypercalciuria, diabetes and urinary tract infections.

Disease	Zn/Ca ratio
Primary hyperparathyroidism	0.0417±0.0082
Hypercalciuria	0.0253±0.008
Diabetes	0.0704±0.0108
Infections	0.0423±0.0078

6. Toward in vivo XRF at the hospital

In the literature, numerous studies (Table 3) have investigated the relationship between the content of trace elements and different diseases [122-188] for different kinds of biological samples. For example, L.M. Marco et al. [130] and C.G.L. Canellas et al. [150] have determined the Zn/Cu ratio in serum samples. D. von Czarnowski et al. [127] have evaluated through total reflection X-ray fluorescence analysis the distribution of trace elements in carcinomas of the digestive tract and in normal tissues of human stomach, colon and rectum in correlation. Finally, XRF offers the possibilities to determine the distribution of Pt based anticancer drugs within tumour and in its proximity [126].

Table 3.
Biological tissues and diseases studied by XRF.

Biological tissues	Aetiology
Hair	Environmental disease [129,152]
Brain	Neurodegenerative diseases [135,131,145,143,144]
Breast	Cancer [139]
Bone	Relation between Pb exposure and memory impairment [124,142]
Cartilage	Environmental disease [137], Arthritis [138]
Gallstones	Environmental [123]
Kidney stones	Environmental [125]
Nails	Environmental [129,146]
Prostate	Cancer [140, 136]
Serums	sickle cell anemia [150]
Skin	body iron burden [131], Environmental [129]
Stomach	Cancer [127]
Tooth enamel	Environmental [129,143]

With the development of X-ray experimental setups [124,134,136,166-188], some investigations have tried to perform in vivo measurements of trace elements such as Fe [187], Au [168], Zn [134,136], Cd [167,171], I [184], Hg [172,181], Pu [188], U[175], Sr [180] and Pb [124,174]. As underlined by several authors, such technique constitutes a safe, rapid, and non-invasive approach. Some of these trace elements namely Au [168] or I [184] are part of drugs or biomedical markers. Gold salts are used in the treatment of rheumatoid arthritis and such XRF experiments allow the clinician to gather information on their mode of action [168]. H. Matsukiyo et al. [184] have developed an XRF camera for carrying out mapping for iodine-based contrast media used in medical angiography. In the case of excessive body toxic elements burdens such as Pb [182], Hg [181] or Cd [167,171], XRF measurements is a practical method for monitoring the efficacy of a therapy as well as for establishing the diagnosis. In vivo XRF experiments have been also collected on kidney [171]. As underlined by U. Nilsson et al. [171], except in the presence of very deeply situated kidneys, where the minimum detectable concentration is high, non-invasive in vivo XRF analysis of kidney cadmium should be a useful tool for evaluating the effects of long-term low-level exposure to cadmium and the risk of kidney damage.

Quite recently, S.S. Shilstein et al. [134, 136] describe a phantom-based feasibility investigation for a potential in vivo determination of zinc in prostate. Such approach is based on several publications which have detailed the compelling evidence and basis for the concept that zinc is involved in the pathogenesis of prostate cancer and that zinc could be efficacious in the prevention and treatment of this cancer [158-161]. Such measurement could bring about improved diagnosis of prostate cancer which is the most common malignancy affecting men and is the second-leading cause of cancer death [162].

Finally, L.H. Nie et al. [186] investigate the methodology and feasibility of developing a portable X-ray fluorescence (XRF) technology to quantify Pb in bone in vivo. The authors report that with such portable XRF device, the detection limit was about 8.4 ppm with 2 mm soft tissue thickness. Also, the entrance skin dose delivered to the human subject was about 13 mSv and the total body effective dose was about 1.5 µSv and should pose minimal radiation risk. They conclude that portable XRF technology can be used for in vivo bone lead measurement with sensitivity comparable to a standard technology. Similar conclusions have been made by M. Estevam and C.R. Appoloni [187] for the assessment of iron levels in patients with thalassemia and hemochromatosis.

7. Conclusion and perspectives

Through these different examples, some of ones being already published, we have clearly demonstrated that in-lab facilities bring significant information to clinicians. Such experimental devices allow the detection of trace elements such Mg, Zn, Fe, Sr or Pb which play major role in medicine [189,190]. Their place in medical research will increase drastically due to major public health problems related to infection and environmental diseases. In the field of kidney stones, a new set of experiments will be dedicated to assess through XRF the relationship between infection and the content of Zn in the stones.

8. Acknowledgments

This research have been performed through scientific discussions with Dr. P.-A. Albouy (LPS) and Dr. E. Foy (Iramis-CEA). This work was supported by the Physics and Chemistry Institutes of CNRS and by contract ANR-09-BLAN-0120-02.

References

[1] G. Sagnac, Thèse, Faculté des sciences de Paris, seconde Partie : rayons secondaires dérivés des rayons de Röntgen, 1900.
[2] M. de Broglie, Compte Rendus de l'académie des sciences 157 (1913) 924.
[3] M. Quintin, J. de Physique IV 6 (1996) C4-599.
[4] R. Jenkins, Anal. Chem. 56 (1984) 1099A.
[5] Guinier A. Théorie et technique de la radiocristallographie, Dunod : Paris; 1964.
[6] B. E. Warren, X-Ray Diffraction, Addison-Wesley, Reading, MA, 1969.
[7] T. R. Welberry, B. D. Butler, Chem. Rev. 95 (1995) 2369.
[8] D. Bazin, D. A. Sayers, J. J. Rehr, J. Phys. Chem. B 101(1997)11040.
[9] C.H. Jones, Phys. Med. Biol. 27 (1982) 463.
[10] R.F. Mould, a century of X-rays and radioactivity in medicine, Institute of Physics Publishing, London, 1993.
[11] D. Krausová, Bulletin of the Czech and Slovak Crystallographic Association 3 (1996) 148.
[12] J. Börjesson, M. Isaksson, S. Mattsson, Acta Diabetol. 40 (2003) S39.
[13] A. Elliott, NIM A 546 (2005) 1.
[13] M. Ralle, S. Lutsenko, Biometals. 22 (2009) 197.
[14] D. Bazin, M. Daudon, J. Phys. D: Appl. Phys. 45 (2012) 383001.
[15] F. Blaske, O. Reifschneider, G. Gosheger, Ch.A. Wehe, M. Sperling, U. Karst, G. Hauschild, S. Höll, Anal. Chem. 86 (2014) 615.
[16] L. Gerhardsson, J. Börjesson, A. Grubb, B. Hultberg, S. Mattsson, A. Schütz, S. Skerfving, Applied Radiation and Isotopes 49 (1998) 711.
[17] D. Bazin, M. Daudon, Ch. Combes, Ch. Rey, Chem. Rev. 112 (2012) 5092.
[18] D. Bazin, J.-Ph. Haymann, E. Letavernier, J. Rode, M. Daudon, La presse médicale 43 (2014) 135.
[19] D. Bazin, M. Daudon, P. Chevallier, S. Rouzière, E. Elkaim, D. Thiaudière, B. Fayard, E. Foy, P.A. Albouy, G. André, G. Matzen, E. Véron, Ann. Biol. Clin. 64 (2006) 125.
[20] K.A. McCall, C.-C. Huang, C.A. Fierke, J. Nutr. 130 (2000) 1437S.
[21] L. Tomljenovic, J. Alzheimers Dis. 23 (2011) 567.
[22] R. P. Csintalan, N. M. Senozan, J. Chem. Educ. 68 (1991) 365.
[23] A. V. Klein, T. W. Hambley, Chem. Rev. 109 (2009) 4911.
[24] A.E. Merbach, E. Toth, The Chemistry of Contrast Agents in Medical Magnetic Resonance Imaging; John Wiley & Sons, Ltd.: New York, 2001.
[25] J. Gao, H. Gu, B. Xu, Acc. Chem. Res. 42 (2009) 1097.
[26] R.L. Sime, Lise Meitner: A Life in Physics, University of California Press, Berkeley (1996).
[27] C. Burggraf, B. Carrière, S. Goldszaub, Revue de Physique Appliquée AA (1976) 13.
[28] C.A. Pineda-Vargas, A.L. Rodgers, M.E. Eisa, Radiation Physics and Chemistry 71 (2004) 947.
[29] C.A. Pineda, M. Peisach, NIM B 85 (1994) 896.
[30] M.A.B. Pougnet, M. Peisach, A.L. Rodgers, NIM B 35 (1988) 472.
[31] I. Abugassa, S.B. Sarmani, S.B. Samat, Applied Radiation and Isotopes 50 (1999) 989.
[32] S. Homma, I. Nakai, S. Misawa, N. Shimojo, NIM B 103 (1995) 229.
[33] D. Bazin, P. Chevallier, G. Matzen, P. Jungers, M. Daudon, Urol Res. 35 (2007) 179.
[34] B. Fayard, M. Salomé, K. Takemoto, H. Kihara, J. Susini, J. of Electron Spectroscopy and Related Phenomena 170 (2009) 19.
[35] W.A. High, J.F. Ranville, M. Brown, T. Punshon, A. Lanzirotti, B.P. Jackson, J. of the American Academy of Dermatology 62 (2010) 38.

[36] S. Bohic, M. Cotte, M. Salomé, B. Fayard, M. Kuehbacher, P. Cloetens, G. Martinez-Criado, R. Tucoulou, J. Susini, J. of Structural Biology 177 (2012) 248.
[37] http://www.nobelprize.org/nobel_prizes/physics/laureates/1915/perspectives.html
[38] X-Ray Diffraction Procedures: For Polycrystalline and Amorphous Materials, 2nd Ed. H.P. Klug, L.E. Alexander, pp. 992. ISBN 0-471-49369-4. Wiley-VCH , May 1974.
[39] A. Le Bail, Mater. Sci. Forum, 378-381 (2001) 65.
[40] A. Le Bail, Powder Diffr. 19 (2004) 249.
[41] A. Le Bail, Powder Diffr. 20 (2005) 316.
[42] Powder diffraction file (PDF), International Centre for Diffraction Data, 12 campus Blvd, Newton square, PA 19073-3273, USA, http://www.icdd.com.
[43] A. Le Bail, D. Bazin, M. Daudon, A. Brochot, V. Robbez-Masson, V. Maisonneuve Acta Cryst. B65 (2009) 350.
[44] M. Daudon, D. Bazin, K. Adil, A. Le Bail, Acta Cryst. E67 (2011) o1458.
[45] A. Le Bail, M. Daudon, D. Bazin, Acta Cryst. C69 (2013) 734.
[46] A. Bellare, R.E. Cohen, Biomaterials 17 (1996) 2325.
[47] M. Niinomi, J. Mech. Behav. Biomed. Mater. 1(2008) 30.
[48] X. Li , C.T. Wang, W.G. Zhang, Y.C. Li, Proc. Inst. Mech. Eng. H. 223 (2009) 173.
[49] K. Fujisaki, S. Tadano, J. Biomech. Eng. 132 (2010) 031004.
[50] T. Nakano, T. Kan, T. Ishimoto, Y. Ohashi, W. Fujitani, Y. Umakoshi, T. Hattori, Y. Higuchi, M. Tane, H. Nakajima, Materials Transactions 47(2006) 2233.
[51] S. Rouzière, E. Jourdanneau, B. Kasmi, P. Joly, D. Petermann, P.A. Albouy, J. Appl. Cryst. 43 (2010) 1131.
[52] A. Randall, N. Engl. J. Med. 214 (1936) 234.
[53] A. Randall, Bull. N. Y. Acad. Med. 20 (1944) 474.
[54] A. Randall, Ann. Surg. 105 (1937) 1009.
[55] A. Randall, J. Urol. 44 (1940) 580.
[56] A.P. Evan, J. Lingeman, F.L. Coe, E. Worcester, Kidney Int. 69 (2006) 1313.
[57] V. Sepe, G. Adamo, A. La Fianza, C. Libetta, M.G. Giuliano, G. Soccio, A. Dal Canton Am. J. of Kidney Diseases 48 (2006) 706.
[58] N.M. Bhuskute, W.W. Yap, T.M. Wah, Eur. J. of Radiology 72 (2009) 470.
[59] D.G. Reid, G.J. Jackson, M.J. Duer, A.L. Rodgers, J. Urol. 185 (2011) 725.
[60] N.L. Miller, J. Urol. 186 (2011) 783.
[61] Th. Chi, J. Miller, M.L. Stoller, Trans. Androl. Urol. 1 (2012) 66.
[62] S.R. Khan, D.E. Rodriguez, L.B. Gower, M. Monga, J. Urol. 187 (2012) 1094.
[63] A. Ciudin, M.P. Luque Galvez, R.S. Izquierdo, M.G. Diaconu, A. Franco de Castro, V. Constantin, J.R. Alvarez-Vijande, C. Nicolau, A.A. Asensio, Urology 81 (2013) 246.
[64] S.D. Blaschko, Th. Chi, J. Miller, S. Fakra, M.L. Stoller, J. Urol. 189 (2013) e849.
[65] M. Daudon, D. Bazin, E. Letavernier, Urolithiasis 43 (2015) 5.
[66] S.C. Kim, F.L. Coe, W.W. Tinmouth, R.L. Kuo, R.F. Paterson, J.H. Parks, L.C. Munch, A.P. Evan, J.E. Lingeman, J. Urol. 173 (2005) 117.
[67] S.R. Khan, B.K. Canales, J. Urol. 186 (2011) 1107.
[68] M. Daudon, O. Traxer, P. Jungers, D. Bazin. In A.P. Evan, J.E. Lingeman, J.C. Williams Jr : Renal Stone Disease. AIP Conf. Proceed., 900 (2007) 26.
[69] M. Daudon, D. Bazin, J. Phys.: Conf. Ser. 425 (2013) 022006.
[70] D.E. Sayers, E.A. Stern, F.W. Lytle, Physical Review Letters 27 (1971) 1204.
[71] F.W. Lytle, D.E. Sayers, E.A. Stern, Phys. Rev B 11 (1975) 4825.
[72] D. Bazin, X. Carpentier, O. Traxer, D. Thiaudière, A. Somogyi, S. Reguer, G. Waychunas,

P. Jungers, M. Daudon, J. Synchrotron Rad. 15 (2008) 506.
[73] D. Bazin, M. Daudon, Ch. Chappard, J. J. Rehr, D. Thiaudière, S. Reguer, J. Synchrotron Rad. 18 (2011) 912.
[74] Ch. Nguyen, H.-K. Ea, D. Thiaudiere, S. Reguer, D. Hannouche, M. Daudon, F. Lioté, D. Bazin, J. Synchrotron Rad. 18 (2011) 475.
[75] D. Bazin, A. Dessombz, Ch. Nguyen, H.K. Ea, F. Lioté, J. Rehr, Ch. Chappard, S. Rouzière, D. Thiaudière, S. Reguer, M. Daudon, J. Synchrotron Rad. 21 (2014) 136.
[76] C.G. Frankaer, A.C. Raffalt, K. Stahl, Calcif. Tissue. Int. 94 (2014) 248.
[77] X. Carpentier, D. Bazin, P. Jungers, S. Reguer, D. Thiaudière, M. Daudon J. Synchrotron Rad. 17 (2010) 374.
[78] X. Carpentier, D. Bazin, Ch. Combes, A. Mazouyes, S. Rouzière, P.A. Albouy E. Foy, M. Daudon, J. Trace Elements Med. Biol. 25 (2011) 160.
[79] D. Bazin, C. Chappard, C. Combes, X. Carpentier, S. Rouzière, G. André, G. Matzen M. Allix, D. Thiaudière, S. Reguer, P. Jungers, M. Daudon, Osteoporos Int. 20 (2009) 1065.
[80] S. Tadano, B. Giri, Sci. Technol. Adv. Mater. 12 (2011) 064708.
[81] S. Sivakumar, C.P. Khatiwada, J. Sivasubramanian, Spectrochimica Acta Part A 126(2014)59.
[82] A. Zamiri, S. De, J. of the mechanical behavior of biomedical materials 4(2011)146.
[83] Y.F. Liu, I. Manjubala, H. Schell, D.R. Epari, P. Roschger, G.N. Duda, P. Fratzl, J. of Bone and Mineral Res. 25 (2010) 2029.
[84] A.K. Mukherjee, J. of the Indian Institue of Science 94 (2014) 35.
[85] V.M. Goldschmitt, J. Chem. Soc. 1 (1937) 655.
[86] T.J. White, D. Zhili, Acta Crystallogr B 59 (2003) 1.
[87] M. Vallet-Regi, M.J. Gonzalez-Calbet, Prog Solid State Chem 32 (2004) 1.
[88] L.N.Y. Wu, B.R. Genge, R.E. Wuthier, J. Inorg. Biochem. 103 (2009) 948.
[89] R.Z. Legeros, C.B. Bleiwas, M. Retino, R. Rohanizadeh, J.P. Legeros, Am. J. Dent 12 (1999) 65.
[90] R.Z. Legeros, D. Mijares, J. Park, X.F. Chang, I. Khairoun, R. Kijkowska, R. Dias, J.P. Legeros, Key Eng Mater 284–286 (2005) 7.
[91] B. Bao, A.S. Prasad, F.W. Beck, Snell D, Suneja A, Sarkar F.H., Doshi N, Fitzgerald, P. Swerdlow, Transl Res.152 (2008) 67.
[92] B. Besecker, S. Bao, B. Bohacova, A. Papp, W. Sadee, D.L. Knoell, Am J Physiol Lung Cell Mol Physiol 294 (2008) L1127.
[93] H. Haase, J.L. Ober-Blobaum, G. Engelhardt, S. Hebel, A. Heit, H. Heine, L. Rink, J. Immunol. 181 (2008) 6491.
[94] M. Daudon, R.J. Réveillaud, Néphrologie 5 (1984) 195.
[95] M. Daudon, C.A. Bader, P. Jungers, Scanning microsc. 7 (1993) 1081.
[96] D. Bazin, X. Carpentier, I. Brocheriou, P. Dorfmuller, S. Aubert, C. Chappard, D. Thiaudière, S. Reguer, G. Waychunas, P. Jungers, M. Daudon, Biochimie 91 (2009) 1294.
[97] C.A. Beevers, Acta Cryst. 11 (1958) 273.
[98] M.J. Glimcher, L.C. Bonar, M.D. Grynpas, W.J. Landis, A.H. Roufosse, J. Crystal Growth 53 (1981) 100.
[99] A. Bigi, M. Gazzano, A. Ripamonti, N. Roveri, J. Inorganic Biochemistry 32 (1988) 251.
[100] J. Redepenning, T. Schlessinger, S. Burnham, L. Lippiello, J. Miyano, J. Biomedical Materials Research 30 (1996) 287.
[101] J. Niu, G. Yuan, Y. Liao, L. Mao, J. Zhang, Y. Wang, F. Huang, Y. Jiang, Y. He, W. Ding, Materials Science and Engineering: C 33(2013)4833.
[102] R. Reyes, B. De la Riva, A. Delgado, A. Hernández, E. Sánchez, C. Évora

Injury 43 (2012) 334.
[103] F. Tamimi, B. Kumarasami, C. Doillon, U. Gbureck, D. Le Nihouannen, E. Lopez Cabarcos, J.E. Barralet, Acta Biomaterialia 4 (2008) 1315.
[104] A.L. Rodgers, M. Spector, Calcif. Tissue Int. 39 (1986) 342.
[105] A.K. Rosenthal, E. Mattson, C.M. Gohr, C.J. Hirschmugl, Osteoarthritis and Cartilage 16 (2008) 1395.
[106] D. Heimbach, D. Jacobs, A. Hesse, S.C. Müller, P. Zhong, G.M. Preminger Urol. Res. 27 (1999) 266.
[107] J.C. Williams Jr., T. Hameed, M.E. Jackson, S. Aftab, A. Gambaro, Y.A. Pishchalnikov, J.E. Lingeman, J.A. McAteer, J. Urol. 188 (2012) 996.
[108] A.E. Krambeck, S.E. Handa, A.P. Evan, J.E. Lingeman, Urol. Res. 38 (2010) 293.
[109] D.L. Miller, N.B. Smith, M.R. Bailey, G.J. Czarnota, K. Hynynen, I.R. Makin J. Ultrasound Med. 31(2012) 623.
[110] D. Ackermann, J. M. Baumann, Urol. Res. 15 (1987) 63.
[111] C.Y.C. Pak, J.R. Poindexter, R.D. Peterson, H.J. Heller, J. Urol.171 (2004) 1046.
[112] R. Siener, L. Netzer, A. Hesse, PLoS ONE 8 (2013) e78996.
[113] H.E. Lundager Madsen, J. Crystal Growth 310 (2008) 2602.
[114] M. Daudon, H. Bouzidi, D. Bazin, Urol. Res. 38 (2010) 459.
[115] M. Daudon, P. Jungers, D. Bazin, N. Engl. J. Med. 359 (2008) 100.
[116] M. Daudon, P. Jungers, D. Bazin, AIP Conf. Proc. 1049 (2008) 199.
[117] M. Daudon, P. Jungers, Urolithiasis, Ed. J.J. Talati, H.-G. Tiselius, D.M. Albala, Z. Ye, (2012) pp 113-140.
[118] A. Dessombz, P. Méria, D. Bazin, M. Daudon PLoS ONE 7(2012)e51691.
[119] A. Dessombz, E. Letavernier, J.-Ph. Haymann, D. Bazin, M. Daudon, J. Urol. 193 (2015) 1564.
[120] M.Y. Donath, Nature Reviews Drug Discovery 13 (2014) 465.
[121] E. Dalmas, N. Venteclef, C. Caer, C. Poitou, I. Cremer, J. Aron-Wisnewsky, S. Lacroix-Desmazes, J. Bayry, S.V. Kaveri, K. Clément, S. André, M. Guerre-Millo, Diabetes. 63 (2014) 1966.
[122] V. Y. Zaichick, T.V. Ṣviridova, S.V. Zaichick, Internat. Urol. Nephrol. 29 (1977) 565.
[123] A.T. Al-Kinani, I.A. Harris, D.E Watt, Phys. Med. Biol. 29 (1984) 175.
[124] V. Batuman, R.P. Wedeen, J.D. Bogden, D.J. Balestra, K. Jones, G. Schidlovsky, Environmental Res. 48 (1989) 70.
[125] S. Galassini, N.Q. Liu, G. Moschini, A. Tasca, G. Villi, V. Valkovic, NIM B 43 (1989) 556.
[126] K.L. Szluha, I. Uzonyi, J. Bacso, L. Lampe, I. Czifra, M. Peter, C. Villena, W. Schmidt Microchemical J. 51 (1995) 238.
[127] D. von Czarnowski, E. Denkhaus, K. Lemke, Spectrochimica Acta Part B 52 (1997) 1047.
[128] L. Benninghoff, D. von Czarnowski, E. Denkhaus, K. Lemke Spectrochimica Acta Part B 52 (1997) 1039.
[129] A.A. Vazina, V.S. Gerasimov, N.P. Gorbunova, P.M. Sergienko, V.M. Shelestov, Y.I. Nesterikhin, V.B. Baryshev, V.K. Zolotaryov, G.N. Kulipanov, V.A. Trunova NIM A 405 (1998) 454.
[130] L.M. Marco, E. Jimenez, E.A. Hernandez, A. Rojas, E.D. Greavese, Spectrochimica Acta Part B 56 (2001) 2195.
[131] M.J. Farquharson, A.P. Bagshaw, Radiation Physics and Chemistry 61 (2001) 599.
[132] E.A. Hernandez-Caraballo, L.M. Marco-Parra, Spectrochimica Acta Part B 58 (2003) 2205.
[133] J. Börjesson, M. Isaksson, S. Mattsson, Acta Diabetologica 40(2003)s39.
[134] S.S. Shilstein, A. Breskin, R. Chechik, G. Feldman, D. Vartsky,

Phys. Med. Biol. 49(2004)485.
[135] A. Ide-Ektessabi, Y. Ota, R. Ishihara, Y. Mizuno, T. Takeuchi, NIM B 241(2005)681.
[136] S.S. Shilstein, M. Cortesi, A. Breskin, R. Chechik, D. Vartsky, G. Raviv, N. Kleinman, J. Ramon,G. Kogan, V. Gladysh, E. Moriel, M. Huszar, A. Volkov, E. Fridman, Talanta 70 (2006) 914.
[137] N. Zoeger, P. Roschger, J.G. Hofstaetter, C. Jokubonis, G. Pepponi, G. Falkenberg, P. Fratzl, A. Berzlanovich, W. Osterode, C. Streli, P. Wobrauschek, Osteoarthritis and Cartilage 14 (2006) 906.
[138] D.A. Bradley, C.J. Moger, C.P. Winlove, NIM A 580(2007) 473.
[139] A. Kubala-Kukuś, D. Banaś, J. Braziewicz, S. Góźdź, U. Majewska, M. Pajek Spectrochimica Acta Part B 62 (2007) 695.
[140] M. Podgórczyk, W.M. Kwiatek, D. Grolimund, C. Borca Radiation Physics and Chemistry 78(2009) S53.
[141] A.C. Leskovjan, A. Lanzirotti, L.M. Miller, NeuroImage 47 (2009) 1215.
[142] E. Van Wijngaarden, J.R. Campbell, D.A. Cory-Slechta, NeuroToxicology 30 (2009) 572.
[143] C. Oprea, P.J. Szalanski, M.V. Gustova, I.A. Oprea, V. Buzguta, Vacuum 83 (2009) S166.
[144] P. Bleuet, L. Lemelle, R. Tucoulou, P. Gergaud, G. Delette, P. Cloetens, J. Susini, A. Simionovici, Trends in Analytical Chemistry 29 (2010) 518.
[145] M.Z. Kastyak, M. Szczerbowska-Boruchowska, D. Adamek, B. Tomik, M. Lankosz, K.M. Gough, Neuroscience 166 (2010) 1119.
[146] M. Katsikini, F. Pinakidou, E. Mavromati, E.C. Paloura, D. Gioulekas, D. Grolimund NIM B 268 (2010) 420.
[147] T. Enomoto, E. Sato, P. Abderyim, A. Abudurexiti, O. Hagiwara, H. Matsukiyo, A. Osawa, M. Watanabe, J. Nagao, S. Sato, A. Ogawa, J. Onagawa, NIM A 635 (2011) 108.
[148] A.C. Leskovjan, A. Kretlow, A. Lanzirotti, R. Barrea, S. Vogt, L.M. Miller NeuroImage 55 (2011) 32.
[149] B. Hannache, A. Boutefnouchet, D. Bazin, M. Daudon, E. Foy, S. Rouzière, A. Dahdouh Prog. Urol. 25 (2015) 22.
[150] C.G.L. Canellas, S.M.F.Carvalho, M.J.Anjos, R.T.Lopes, Applied Radiation and Isotopes70 (2012) 1277.
[151] S. Khanna, A.C. Udas, G. Kiran Kumar, S. Suvarna, F.R. Karjodkar J. of Trace Elements in Medicine and Biology 27 (2013) 307.
[152] K.S. Ali Aldroobi, A. Shukri, S. Bauk, E.M. Abdel Munem, A.M.A. Abuarra Rad. Phys. and Chem. 91 (2013) 9.
[153] W. Zheng, H. Nichol, S. Liu, Y.-Ch.N. Cheng, E.M. Haacke, NeuroImage 78 (2013) 68.
[154] A. Daoust, E.L. Barbier, S. Bohic, NeuroImage 64 (2013) 10.
[155] A. Mersov, G.Mersov, A.Al-Ebraheem, S.Cornacchi, G.Gohla, P.Lovrics, M.J. Farquharson, Radiation Physics and Chemistry 95 (2014) 210.
[156] R.G. Leitão, A. Palumbo Jr., P.A.V.R. Souza, G.R. Pereira, C.G.L. Canellas, M.J. Anjos, L.E. Nasciutti, R.T. Lopes, Radiation Physics and Chemistry 95 (2014) 62.
[157] J.C.A.C.R. Soares, C.G.L. Canellas, M.J. Anjos, R.T. Lopes, Radiation Physics and Chemistry 95 (2014) 317.
[158] L.C. Costello, R.B. Franklin, Prostate 35(1998) 285.
[159] L.C. Costello, R.B. Franklin, Oncology 59 (2000) 269.
[160] L.C. Costello, R.B. Franklin Oncol Spectr 2 (2001) 452.
[161] L.C. Costello, P. Feng, B. Milon, M. Tan, R.B. Franklin, Prostate Cancer and Prostatic Diseases 7 (2004) 111.

[162] E.D. Crawford, Urology 6 (2003) 3.
[163] A. Grubman, S.A. James, J. James, C. Duncan, I. Volitakis, J.L. Hickey, P.J. Crouch, P.S. Donnelly, K.M. Kanninen, J.R. Liddell, S.L. Cotman, M.D. de Jonge, A.R. White Chem. Sci. 5 (2014) 2503.
[164] L. Yang, R. McRae, M.M. Henary, R. Patel, B. Lai, S. Vogt, Ch.J. Fahrni, PNAS 102 (2005) 11179.
[165] Y. Yuan, S. Chen, S.C. Gleber, B. Lai, K. Brister, C. Flachenecker, B. Wanzer, T. Paunesku, S. Vogt, G.E. Woloschak, J. Phys.: Conf. Ser. 463 (2013) 012020.
[166] L. Ahlgren, K. Liden, S. Mattsson, S. Tejning, Scand. J. Work Environment Health 2 (1976) 82.
[167] L. Ahlgren, S. Mattsson, Physics in Medicine and Biology 26 (1981) 19.
[168] J. Shakeshaft, A.K. Clarke, M.J. Evans, S.C. Lillicrap, Basic Life Sciences 60 (1993) 307.
[169] A.C. Todd, D.R. Chettle, Environ Health Perspect. 102 (1994) 172.
[170] D.G. Lewis, Phys. Med. Biol. 39 (1994) 197.
[171] U. Nilsson, A. Schütz, S. Skerfving, S. Mattsson, Internat. Archives of Occupational and Environmental Health 67 (1995) 405.
[172] Böerjesson, J., 1996. Studies of cadmium, mercury and lead in man: the value of x-ray fluorescence measurements in vivo. PhD Thesis, Lund University, Malmö, Sweden.
[173] P. A. Ali, C. Bennet, A. M. EL-Sharkawi, D. A. Hancock Appl. Radiat. Isot. 49 (1998) 647.
[174] V. Zaichick, N. Ovchjarenko, S. Zaichick, Applied Radiation and Isotopes 50 (1999) 283.
[175] O'Meara, J.M. 1999. Measuring lead, mercury, and uranium by in vivo x-ray fluorescence. PhD Thesis, McMaster, University, Hamilton, ON, Canada.
[176] Th.M. Ambrose, M. Al-Lozi, M.G. Scott, Clinical Chemistry 46 (2000) 1171.
[177] J.M. O'Meara, J. Börjesson, D.R. Chettle, Applied Radiation and Isotopes 53 (2000) 639.
[178] S.H. Lee, R.P. Gardner, A.C. Todd, Appl Radiat Isot. 54 (2001) 893.
[179] J. Börjesson, M. Isaksson, S. Mattsson, Acta Diabetologica 40 (2003) s39.
[180] A. Pejović-Milić, I. M. Stronach, J. Gyorffy, C. E. Webber, D. R. Chettle Med. Phys. 31 (2004) 528.
[181] J.M. O'Meara, J. Börjesson, D.R. Chettle, F.E. McNeill, NIM B 213 (2004) 560.
[182] H. Nie, D. Chettle, L. Luo, J. O'Meara, NIM B 263 (2007) 225.
[183] H. Nie,H. Hu, D.R. Chettle, X-Ray Spectrom.37 (2008) 69.
[184] H. Matsukiyo, M. Watanabe, E. Sato, A. Osawa, T. Enomoto, J. Nagao, P. Abderyim, K. Aizawa, E. Tanaka, H. Mori, T. Kawai, S. Ehara, S. Sato, A. Ogawa, J. Onagawa Radiological Physics and Technology 2 (2009) 46.
[185] D.R. Chettle, Pramana 76 (2011) 249.
[186] L.H. Nie, S. Sanchez, K. Newton, L. Grodzins, R.O. Cleveland , M.G. Weisskopf Phys. Med. Biol. 56 (2011)N39.
[187] M. Estevam, C.R. Appoloni, Health Phys. 104 (2013) 132.
[188] H. Yoshii, K. Yanagihara, H. Imaseki, T. Hamano, H. Yamanishi, M. Inagaki, Y. Sakai, N. Sugiura, O. Kurihara, K. Sakai, PLoS ONE 9 (2014) e101966.
[189] V.K. Singh, P .K. Rai, Biophysical Reviews 6 (2014) 291.
[190] L. Louvet, D. Bazin, J. Büchel, S. Steppan, J. Passlick-Deetjen, Z.A. Massy PloS ONE 10 (2015) e0115342.